Hysteresis and Its Model Prediction of Electrorheological Fluids

Young Dae Kim
Faculty of Applied Chemistry, Chonnam National University, Kwangju 500–757, Korea

Daniel De Kee
Dept. of Chemical and Biomolecular Engineering and Tulane Institute for Macromolecular Engineering and Science (TIMES), Tulane University, New Orleans, LA 70118

DOI 10.1002/aic.10871
Published online April 21, 2006 in Wiley InterScience (www.interscience.wiley.com).

Electrorheological (ER) fluids are suspensions of polarizable particles dispersed in insulating liquids. They exhibit a rapid and reversible transition from a liquid-like to a solid-like state upon the application of an electric field. The observed shear stress–shear rate hysteresis makes the precise control of the ER mechanical devices very difficult. Hysteresis behavior of TiO_2 ER fluids were observed by varying particle concentration, electric field strength, maximum shear rate, and the time of the hysteresis loop. In the absence of an electric field, the stress level of the up curve exceeds that of the down curve. The presence of an electric field reverses this trend. The extent of hysteresis becomes more significant with increasing electric field strength, particle concentration, and maximum shear rate. Hysteresis behavior of TiO_2 ER fluids seems to arise mainly due to the change of the particle structure during shearing. To describe the complex rheological behavior of ER fluids, a kinetic theory is presented. Model predictions show qualitative agreement with the experimental hysteresis data. © 2006 American Institute of Chemical Engineers *AIChE J,* 52: 2350–2355, 2006
Keywords: electrorheological fluid, hysteresis

Introduction

Electrorheological (ER) fluids are suspensions of polarizable particles dispersed in insulating liquids. They exhibit a rapid and reversible transition from a liquid-like to a solid-like state upon the application of an electric field. The ER phenomena arise from the changes in the particle structures, aligning into a fibrous structure in the direction of the field due to electrostatic forces. The ER effects can potentially be suitable for various engineering applications, such as dampers, clutches, and adaptive structures.[1,2]

ER fluids exhibit a rather complex rheological behavior, such as yield stress, shear thinning, and thixotropy. This depends on the combination of particles and liquids and the applied electric field strength. The shear stress–shear rate hysteresis makes the precise control of ER mechanical devices very difficult[3] and may cause inevitable degeneration of control performance associated with the lack of actuator position accuracy, for example.[4] In this regard, the information and prediction of the hysteresis behavior of ER fluids would be very helpful.

Hysteresis behavior in ER fluids was reported for ER suspensions of organic particles.[4-6] Hysteresis was considered to be related to the loss rate of chain structure caused by the applied shear and to the rate of structure build-up by an applied electric field.[5] Aizawa et al.[6] associated the hysteresis in ER fluids to different extents of cluster breaking and lamellae formations. Following hysteresis measurements, they observed particle agglomeration. Field-dependent hysteresis was also observed for polymethylaniline-based ER fluids.[4]

Correspondence concerning this article should be addressed to D. D. Kee at ddekee@tulane.edu.

Concentrated suspensions, polyelectrolytes, biological fluids, and many other fluids widely used in industry exhibit very complex rheological properties, such as (anti)-thixotropy, shear thinning, shear thickening, and viscoelasticity. Various models have been proposed to describe such complex rheological properties. Many current theories are either too complicated or unable to effectively describe material behavior for a variety of flow situations in terms of a realistic number of model parameters. Soong and Shen[7] and Liu et al.[8] proposed a structural model in which they related the viscosity change to shear-induced structural breakdown. This was further developed by De Kee and Chan Man Fong,[9,10] to include shear-induced structural buildup and to be able to describe the behavior of complex structural fluids.

Here we look at the applicability of this proposed kinetic approach for describing the complex rheological behavior of ER fluids, especially hysteresis behavior. Hysteresis behavior of TiO_2 ER fluids was observed by varying particle concentration, electric field strength, maximum shear rate, and the time of execution of the hysteresis loop. Model predictions are compared to the experimental hysteresis data.

Experimental Procedures

ER fluids were prepared by dispersing TiO_2 (Aldrich, ~325 mesh) particles in silicone oil (Fluka, $\eta_c = 100$ cP, $\rho_c = 0.967$ g/cm^3). The suspensions were allowed to equilibrate for at least 3 days prior to performing the experiments.

The experiments were performed at 25°C using a TA Instrument AR-2000 rheometer fitted with parallel plates, and modified for the application of large electric fields. Potential differences were supplied via a high-voltage d.c. power supply (Glassman High Voltage Inc). Samples were placed between the parallel plates and sheared for 1 min at a (large) shear rate of ~80 s^{-1} and zero field strength to ensure a uniform particle distribution. The desired electric field was then applied for 1 min under zero shear prior to the measurements. Experiments were performed with increasing shear rates to obtain the steady shear viscosity and primary normal stress differences as a function of shear rate. In a hysteresis loop experiment, the shear rate $\dot{\gamma}$ is linearly increased from zero to a maximum value $\dot{\gamma}_m$ and then linearly decreased from $\dot{\gamma}_m$ to zero in a time of $2t_o$. The corresponding shear stress τ is measured.

Theory

A first order kinetic model previously introduced by De Kee and Chan Man Fong[10] is used to describe the rheological properties of the ER fluids. Next we briefly review the approach. The rheological properties depend on n, a structural parameter that represents the number density of structural units associated with the ER fluid. The structural changes in the ER fluids arise from the interaction of the hydrodynamic force, due to the applied shear, and the electrostatic force, due to the applied electric field.[11] When an ER fluid is deformed under an applied electric field, the structure changes and the rate of change of n can be written as

$$\frac{dn}{dt} = k_c(n_o - n) + k_1 n f_2 - k_1 n f_1 \tag{1}$$

where k_c, k_1, and k_l are constants; n_o is the initial number of "structural elements"; and f_1 and f_2 are functions of a macroscopic variable such as, for example, the second invariant of the rate-of-deformation tensor. The first two terms on the right side refer to a structural buildup due to the electrostatic force, diffusion, and deformation, respectively. The last term accounts for the loss rate of structure due to deformation. This continuum mechanics approach is very flexible in that different choices for the functions f_1 and f_2 are possible.

Equation 1 describes the structural changes of the ER fluid. In addition, we need to introduce a constitutive equation relating the macroscopic dynamic variables to the kinetic variables. ER fluids, as many complex structured fluids, exhibit viscoelastic properties.[12,13]

To describe the viscoelastic behavior of an ER fluid, a generalized Maxwell model is introduced as follows[9]:

$$\underline{\underline{\tau}} + \lambda_m \hat{\underline{\underline{\tau}}} = \eta_m \underline{\underline{\dot{\gamma}}} \tag{2}$$

where $\underline{\underline{\tau}}$ and $\underline{\underline{\dot{\gamma}}}$ are the stress and rate-of-deformation tensors, respectively, and λ_m and η_m are functions of the structural parameter n. $\hat{\underline{\underline{\tau}}}$ is the Gordon-Schowalter derivative of $\underline{\underline{\tau}}$, and is given by

$$\hat{\underline{\underline{\tau}}} = \frac{\partial \underline{\underline{\tau}}}{\partial t} + (\underline{v} \cdot \underline{\nabla})\underline{\underline{\tau}} - (\underline{\underline{\nabla v}}) \cdot \underline{\underline{\tau}} - \underline{\underline{\tau}} \cdot (\underline{\underline{\nabla v}})^T + \frac{a}{2}[\underline{\underline{\tau}} \cdot \underline{\underline{\dot{\gamma}}} + \underline{\underline{\dot{\gamma}}} \cdot \underline{\underline{\tau}}] \tag{3}$$

where $\underline{v}$ is the velocity and a is a slip parameter. The upper/lower Oldroyd convected derivatives and the Jauman derivative are obtained by setting a equal to zero, two, and one, respectively.

The solution of Eq. 1, subject to the initial condition $n = n_o$ at $t = 0$, yields:

$$\hat{n}(t) = e^{-H(t)}\left(1 + k_c \int_0^t e^{H(x)} dx\right) \tag{4}$$

where $H(t) = \int_0^t \alpha_o d\xi$ with $\alpha_o = k_c(1 + bf_1 - cf_2) = k_c[1 + (k_l/k_c)f_1 - (k_1/k_c)f_2]$. Assuming the viscosity $\eta(\dot{\gamma}, t)$ to be proportional to n, the transient viscosity after the onset of the shear ($\dot{\gamma}$) is given by:

$$\eta(\dot{\gamma}, t) = \eta_o \frac{n}{n_o} = \eta_o \hat{n}(t) = \eta_o e^{-H(t)}\left(1 + k_c \int_0^t e^{H(x)} dx\right) \tag{5}$$

where η_o is the "constant" zero shear viscosity. Equation 5 reduces to:

$$\eta(\dot{\gamma}, t) = \frac{\eta_o k_c}{\alpha_o}[1 + (bf_1 - cf_2)e^{-\alpha_o t}] \tag{6}$$

when $\dot{\gamma}$ is independent of time.

The steady shear viscosity is then given by:

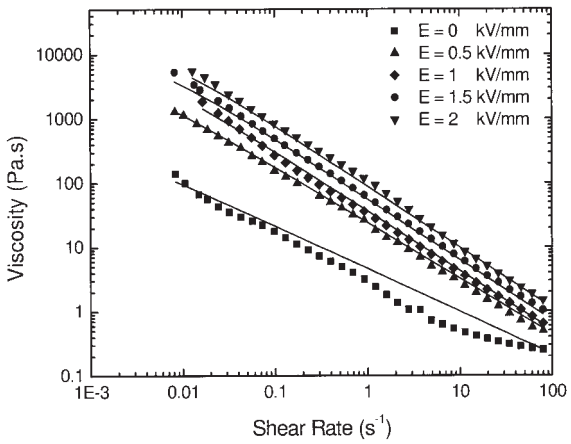

Figure 1. Steady shear viscosity as a function of shear rate for a 20 wt.% TiO_2 ER fluid at different electric field strengths.

—: Predictions of Eq. 8.

$$\eta(\dot{\gamma}) = \frac{\eta_o}{1 + bf_1 - cf_2} \tag{7}$$

We choose to define f_1 and f_2 as rational functions of $\dot{\gamma}$, such that

$$\eta(\dot{\gamma}) = \frac{\eta_o}{1 + \beta\dot{\gamma}^m} \tag{8}$$

where β and m are constants. The parameters η_o, β, and m can be determined by fitting Eq. 8 to the steady shear viscosity–shear rate data.

In simple shear flow, the steady shear viscosity $\eta(\dot{\gamma})$, and the primary and secondary normal stress coefficients Ψ_1 and Ψ_2 can be derived from Eqs. 2 and 3 and are given by[14]:

$$\eta(\dot{\gamma}) = \frac{\tau_{yx}}{\dot{\gamma}} = \frac{\eta_m}{1 + a(2 - a)\lambda_m^2\dot{\gamma}^2} \tag{9}$$

$$\Psi_1(\dot{\gamma}) = 2\lambda_m\eta(\dot{\gamma}) \tag{10}$$

$$\Psi_2(\dot{\gamma}) = -a\lambda_m\eta(\dot{\gamma}) \tag{11}$$

The value of Ψ_2 is difficult to obtain and is usually small. In the case where $a = 0$ it follows that

$$\eta_m = \eta \tag{12}$$

λ_m can be determined from η and Ψ_1, which can be written as a rational function of $\dot{\gamma}$:

$$\Psi_1(\dot{\gamma}) = \frac{\Psi_o}{1 + \alpha\dot{\gamma}^r} \tag{13}$$

where α and r are constants.

Substituting η_m and λ_m into Eq. 2, we obtain the shear stress τ.

$$\tau = \frac{\eta_0}{e^{G(t)}} \int_0^t \left\{ g(x)e^{G(x)-H(x)} \left[1 + k_c \int_0^x e^{H(\xi)}d\xi \right] \dot{\gamma}(x) \right\} dx \tag{14}$$

where $G(t) = \int_0^t g(\xi)d\xi$, $g(x) = 1/\lambda_m$.

For $\lambda_m = 0$ (that is, no elasticity), Eq. 14 reduces to

$$\tau = \frac{\eta_0}{e^{H(t)}} \left[1 + k_c \int_0^t e^{H(\xi)}d\xi \right] \dot{\gamma}(t) \tag{15}$$

Results and Discussion

Steady viscometric data

Figures 1 and 2 show steady shear viscosity–shear rate data and primary normal stress coefficient–shear rate data, as well as model predictions of Eqs. 8 and 13, respectively, at different electric field strengths for a 20 wt.% TiO_2 ER fluid. Table 1 lists the obtained model parameters for the 10 and 20 wt.% TiO_2 ER fluids.

In the absence of an electric field, both the 10 and 20 wt.% TiO_2 ER fluids showed no appreciable primary normal stress differences. In the presence of an electric field, the TiO_2 ER fluids exhibited apparent negative primary normal stress differences at all shear rates (up to 80 s^{-1}) in our experiments. The magnitudes of the negative primary normal stress differences decrease with increasing electric field strength. The negative primary normal stress differences are due to an electrostatic attractive force between the electrodes and the stress increases are due to an induced particle network.[12] To obtain just the electrically induced primary normal stress difference increments as a function of shear rate, the measured primary normal stress difference data were adjusted by considering the effect of the electrostatic attractive force.

Figure 3 shows shear stress–shear rate hysteresis curves for

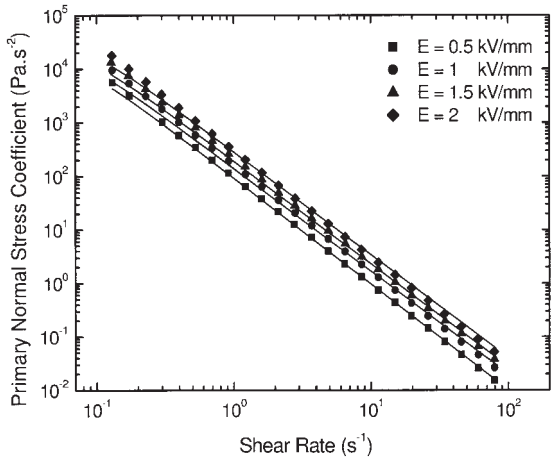

Figure 2. Steady primary normal stress difference as a function of shear rate for a 20 wt.% TiO_2 ER fluid at different electric field strengths.

—: Predictions of Eq. 13.

Table 1. Model Parameters of Eqs. 8 and 13 for 10 and 20 wt.% TiO_2 ER Fluids

Electric Field (V/mm)	Parameters	10 wt.% TiO_2 ER Fluids	20 wt.% TiO_2 ER Fluids
0	η_o (Pa · s)	50	1400
	β	40	300
	m	0.6	0.67
500	η_o (Pa · s)	700	9500
	β	130	330
	m	0.9	0.87
	Ψ_o (Pa · s^{-2})	2100	28500
	α	110	310
	r	1.91	1.91
1000	η_o (Pa · s)	1900	13000
	β	165	300
	m	0.93	0.93
	Ψ_o (Pa · s^{-2})	5700	39000
	α	150	280
	r	1.93	1.92
1500	η_o (Pa · s)	3200	14000
	β	190	250
	m	0.94	0.945
	Ψ_o (Pa · s^{-2})	9600	42000
	α	150	220
	r	1.92	1.92
2000	η_o (Pa · s)	6220	18000
	β	250	225
	m	0.96	0.95
	Ψ_o (Pa · s^{-2})	18600	54000
	α	170	190
	r	1.91	1.91

a 20 wt.% TiO_2 ER fluid at E = 1500 V/mm, for t_o values of 25, 50, and 100 s, and $\dot{\gamma}_m$ is 20 s^{-1}. For all values of t_o, the stress associated with the up curves is lower than for the down curves and the change in t_o does not influence the extent of hysteresis; that is, the areas described by the hysteresis loops are almost comparable. The magnitudes of the stress increase with increasing t_o.

Figure 4 shows shear stress–shear rate hysteresis behavior for a 20 wt.% TiO_2 ER fluid at E = 1500 V/mm, for $\dot{\gamma}_m$ values of 20, 30, and 40 s^{-1} and t_o = 50 s. For all values of $\dot{\gamma}_m$, the

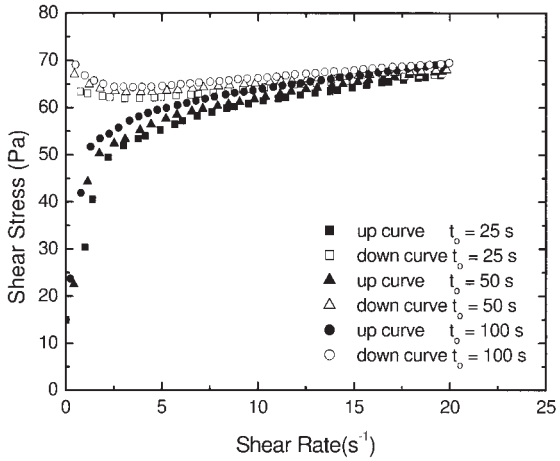

Figure 3. Shear stress–shear rate hysteresis of a 20 wt.% TiO_2 ER fluid at E = 1.5 kV/mm.

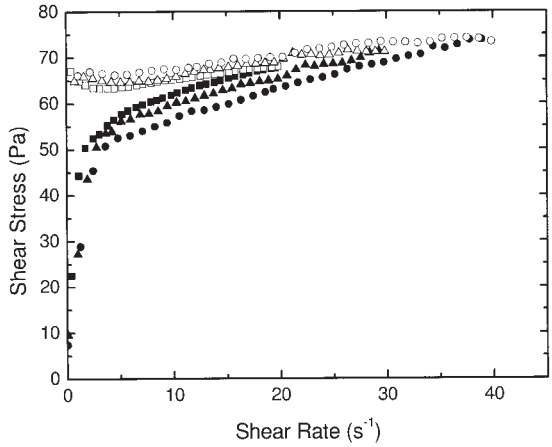

Figure 4. Shear stress–shear rate hysteresis of a 20 wt.% TiO_2 ER fluid at E = 1.5 kV/mm.

t_o = 50 s. The open symbols refer to the down curves.

stress values in the down curves exceed those in the up curves. The transient behavior becomes more significant with increasing $\dot{\gamma}_m$, and as a result, the extent of hysteresis increases.

Hysteresis prediction

In a hysteresis experiment, the shear rate $\dot{\gamma}$ is linearly increased at a constant rate $\dot{\gamma}_c$ from zero to a maximum value $\dot{\gamma}_m$ and then linearly decreased at the same rate to zero in a time of $2t_o$. This is expressed as:

$$\dot{\gamma} = \begin{cases} \ddot{\gamma}_c, & 0 \le t \le t_o \\ \dot{\gamma}_m - \ddot{\gamma}_c(t - t_o), & t_o \le t \le 2t_o \end{cases} \tag{16}$$

Model predictions for the hysteresis behavior of ER fluids are via Eq. 14. The model describes hysteresis loops in terms of seven parameters: η_o, β, m, Ψ_o, α, r, and k_c. The first three parameters are determined via the viscosity–shear rate data and

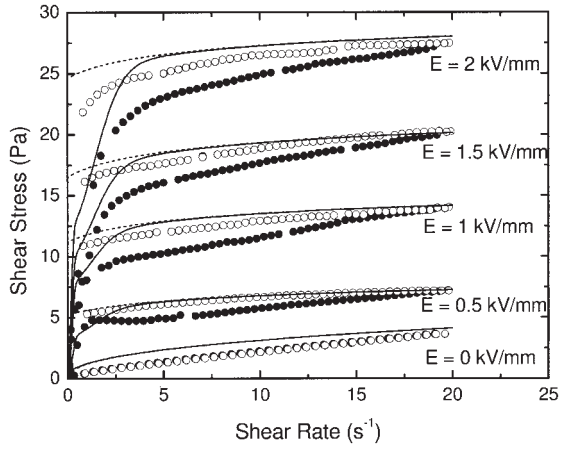

Figure 5. Shear stress–shear rate hysteresis of a 10 wt.% TiO_2 ER fluid at different electric field strengths.

●: Up curve, ○: down curve; model predictions: —: up curve, ---: down curve.

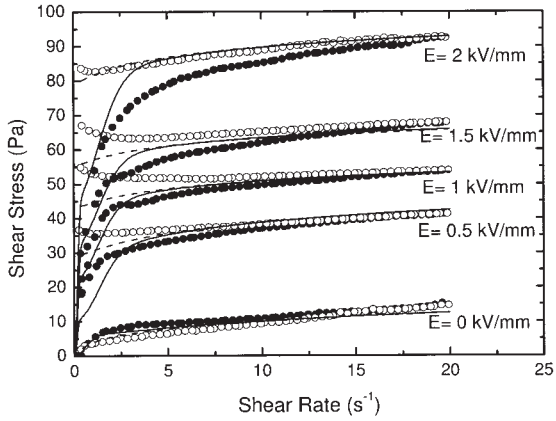

Figure 6. Shear stress–shear rate hysteresis of a 20 wt.% TiO_2 ER fluid at different electric field strengths.

● : Up curve, ○: down curve; model predictions : —: up curve, --- : down curve.

Eq. 8. Three other parameters (Ψ_o, α, and r) are determined via the steady primary normal stress coefficient data and Eq. 13.

Figure 5 shows the experimental and predicted hysteresis curves for a 10 wt.% TiO_2 ER fluid. The shear rate $\dot{\gamma}$ is linearly increased from zero to a maximum value $\dot{\gamma}_m$ of 20 s^{-1} and then linearly decreased from $\dot{\gamma}_m$ to zero in a time of $2t_o$, where t_o is 25 s. In the absence of an electric field, the ER fluid shows very small, almost insignificant, hysteresis and the up curve (increasing rate) is associated with larger stress values than the down curve. With the application of an electric field, the hysteresis behavior is significant and changes; that is, the down curves achieve larger stress values than the up curves for all electric fields. Also, the extent of hysteresis becomes more significant with increasing electric field strength. That is to say, the area between the up and down curves increases.

When E = 0, no primary normal stress differences were observed (that is, λ_m is zero) and Eq. 15 was used to predict the hysteresis. The value of k_c was determined to be 0.18 in the presence of an applied electric field and 1 in the absence of an electric field. The model qualitatively predicts larger stress values for the down curve as well as an increasing extent of hysteresis with increasing electric field strength. In the absence of an electric field, the model also predicts the insignificant hysteresis behavior.

Figure 6 shows the experimental and predicted hysteresis curves for a 20 wt.% TiO_2 ER fluid. The values for $\dot{\gamma}_m$ and t_o are as in Figure 5. Again, when E = 0, no primary normal stress differences were observed (that is, λ_m is zero) and Eq. 15 was used to predict the hysteresis. In the absence of an electric field, the model qualitatively predicts the hysteresis behavior (larger stress values for the up curve) as for the 10 wt. % case. In the presence of an electric field, the model qualitatively predicts the larger stress values for the down curve as well as the increasing extent of hysteresis with increasing electric field strength. The value of k_c was determined to be 0.18 in the presence of an applied electric field and 0.006 in the absence of an electric field.

To our knowledge, no other hysteresis predictions are available in the literature.

Comparing Figures 5 and 6, we observe that the extent of hysteresis increases with increasing particle concentration. The hysteresis dependence on particle concentration was also observed by Hyun et al.[15] Also, the stress overshoot in the up curve decreases and the shape of the up curve becomes more parabolic with increasing electric field strength. The first part (on the up curve) of the hysteresis behavior is associated with elastic behavior of the sample. At the same time, the viscous behavior can become apparent in the first tendency to flatten out.[15] With increasing electric field strength, ER fluids become more elastic and, as a result, the stress in the hysteresis up curve increases to generate a more parabolical curve.

In the absence of an electric field, the down curve is associated with lower stress values than the up curve. Without an applied electric field, ER fluids become more viscous, leading to an easier structural breakdown during the up curve part of the experiment. The restoration of structure takes place slowly during the second half (down curve) of the experiment, leading to smaller stress values.

Thixotropy becomes significant when the characteristic time of the fluid becomes significantly larger than the characteristic time of the flow, that is, when the elastic properties of the fluid gain importance.[16] The increasing extent of hysteresis arises from the increasing elastic properties of ER fluids with increasing electric field strength. Aizawa et al.[6] reported that the larger stress values of the down curve were due to different extents of cluster breaking and lamellae formations. However, in our experiments, we did not observe any lamellae formation during the hysteresis experiment and we postulate that the phenomenon arises mainly due to cluster formation, that is, due to the change of particle structure during shear. Filisko et al.[17] reported that under the simultaneous stimulus of an electric field and shear, the particle chains aligned in tightly packed geometric structures consistent with the flow field. In this case, shear dissipation is not associated with chain breaking but by the structures maintaining their integrity and by shearing within the structures. Shearing flocculated suspensions can densify individual flocs, causing a reorganization within the flocs.[17] Thus, the magnitudes of the stress in the down curve exceed that of the up curve in the presence of an electric field due to a reorganization of particle chains, which maintain their integrity during shearing.

Conclusions

ER fluids, as well as other structured materials, exhibit rather complex rheological behavior, such as yield stress, shear thinning, and thixotropy, which depend on the combination of particles and liquids and on the applied electric field strength. The observed hysteresis behavior renders the precise control of ER mechanical devices rather difficult.

The hysteresis behavior of TiO_2 ER fluids was determined by varying particle concentration, electric field strength, maximum shear rate, and the time of the hysteresis loop. In the absence of an electric field, the stress values of the up curve are larger than those of the down curve. This situation is reversed in the presence of an electric field. The extent of hysteresis becomes more significant with increasing electric field strength, particle concentration, and maximum shear rate at a fixed hysteresis loop time. It is almost independent of the time of hysteresis loop. Hysteresis behavior of TiO_2 ER fluids seems

to arise mainly as a result of cluster formation, that is, the change of the particle structure during shearing.

To predict the hysteresis behavior of ER fluids, a kinetic theory approach proposed earlier for describing the rheological properties of structured fluids is employed. Model predictions are in qualitative agreement with experimental hysteresis data.

Acknowledgments

DDK gratefully acknowledges financial support via NASA grant NCC3–946.

Literature Cited

1. Hartsock DL, Novak RF, Chaundy GJ. ER fluid requirements for automotive devices. *J Rheol.* 1991;35:1305-1326.
2. Block H, Kelly P. Electro-rheology. *J Phys D: Appl Phys.* 1988;21: 1661-1677.
3. Bullough WA. Miscellaneous electro-rheological phenomena—Part I. Proceedings of the 2nd International Conference on ER Fluids, Carlson JD, Sprecher AF, Conrad H. Eds.; Lancaster, PA: Technomic Publishing Co. 1989:115-123.
4. Han YM, Lim SC, Lee HG. Choi SB, Choi HJ. Hysteresis identification of polymethylaniline-based ER fluid using Preisach model. *Mater Design.* 2003;24:53-61.
5. Choi HJ, Jhon MS. Hysteresis behavior of poly(naphthalene quinone) radical electrorheological fluid. *Int J Mod Phys B.* 1999;13:1901-1907.
6. Aizawa R, Vieira SL, Nakano M. Hysteresis phenomena in flow-curve of ER fluids containing sulfonated polymer particles. Proceedings of the 7th International Conference on ER Fluids and MR Suspensions, Tao R. Ed.; Hackensack, NJ: World Scientific Publishing Co. 1999: 595-602.
7. Soong D, Shen M. Shear-rate dependent viscosity of non-Newtonian suspensions and entangled polymer systems. *Polym Eng Sci.* 1980;20: 1177-1180.
8. Liu T, Soong D, De Kee D. A model for structural fluids. *Chem Eng Commun.* 1983;22:273-285.
9. De Kee D, Chan Man Fong CF. Rheological properties of structured fluids. *Polym Eng Sci.* 1994;34:438-445.
10. De Kee D, Chan Man Fong CF. Elongation, hysteresis, and oscillatory flows of complex fluids. *Polym Eng Sci.* 1995;35:1031-1036.
11. Parthasarathy M, Klingenberg DJ. Electrorheology: mechanisms and models. *Maters Sci Eng.* 1996;R17:57-103.
12. Minagawa K, Kimura H, Takimoto J, Koyama K. Electrorheological normal stress measurements of polymer solutions and suspensions. *Int J Mod Phys B.* 1996;10:3237-3242.
13. Yang IK, Elongational flow of a liquid crystalline polymer solution under a transverse electric field. *J Rheol.* 2000;46:1-10.
14. Carreau PJ, De Kee D, Chhabra RP. *Rheology of Polymeric Systems: Principles and Applications*. New York: Hanser/Gardner; 1997.
15. Hyun YH, Lim ST, Choi HJ, Jhon MS. Rheology of poly(ethylene oxide)/organoclay nanocomposites. *Macromolecules*. 2001;34:8084-8093.
16. Barnes HA. Thixotropy—a review. *J Non-Newtonian Fluid Mech.* 1997;70:1-33.
17. Filisko FE., Henley S, Quist G. Recent development in the properties and composition of ER fluids. Proceedings of the 4th International Conference on Intelligent Materials ICIM '98, Makuhari, Chiba, Japan. T. Takagi, M. Aizawa, T. Okano and N. Shinya, Eds.; 1998:114-117.

Manuscript received July 25, 2005, and revision received Mar. 10, 2006.